Acta Oceanol. Sin., 2020, Vol. 39, No. 1, P. 63–73
https://doi.org/10.1007/s13131-019-1528-x
http://www.hyxb.org.cn
E-mail: hyxbe@263.net

Seasonal linkage of the Southern Hemisphere extratropical climate variability to two types of ENSO

Zhongpeng Wang[1], Zhaoru Zhang[1]*, Meng Zhou[1], Hailong Liu[1], Yisen Zhong[1], Xiaoqiao Wang[1]

[1] Institute of Oceanography, Shanghai Jiao Tong University, Shanghai 200240, China

Received 28 October 2018; accepted 25 February 2019

Abstract

This study uses the Climate Forecast System Reanalysis (CFSR) to investigate the responses of the Southern Hemisphere (SH) extratropical climate to two types of El Niño–Southern Oscillation (ENSO)—the eastern Pacific (EP) type and the central Pacific (CP) type in different seasons. The responses are denoted by the anomalies of climate variables associated with one-standard-deviation increase in the Niño3 or Niño4 index. The results show that in austral spring the differences in the ENSO-related anomaly (ERA) patterns of atmospheric circulation between the EP ENSO period (1979–1998) and CP ENSO period (1999–2010) are mainly associated with the change in the ENSO-PSA2 relationship. Such differences affect the ERA fields of surface air temperature and mixed layer temperature, and finally result in significant differences in sea-ice concentration anomalies in the Atlantic sector. In austral summer, significant correlation exists between the variations of SAM and both of the variations of Niño3 and Niño4 in 1979–1998, while the correlation between SAM and Niño4 disappears in 1999–2010. For all seasons, the strength of the climate ERAs depend on if there are close relationship between ENSO and the major climate variation modes of the SH extratropics. For the climate variables, the ERA patterns of surface air temperature are generally controlled by surface wind anomalies and mirrored by the mixed layer temperature anomalies. The mixed layer depth anomalies are primarily modulated by surface heat flux anomalies and occasionally by anomalous wind. There are strikingly strong anomalies of surface heat flux in the autumn of 1979–1998 related to the Niño3 variation, the period when there is only significant correlation between ENSO and PSA2. There are no evidence that the SH extratropical climate variability induced by Niño3 variations are stronger in the EP-ENSO period, and that variability induced by Niño4 variations are stronger in the CP-ENSO period.

Key words: Southern Hemisphere, extratropical climate, El Niño–Southern Oscillation, eastern Pacific type, central Pacific type

Citation: Wang Zhongpeng, Zhang Zhaoru, Zhou Meng, Liu Hailong, Zhong Yisen, Wang Xiaoqiao. 2020. Seasonal linkage of the Southern Hemisphere extratropical climate variability to two types of ENSO. Acta Oceanologica Sinica, 39(1): 63–73, doi: 10.1007/s13131-019-1528-x

1 Introduction

ENSO is a dominant climate mode related to coupled atmospheric and oceanic processes over the tropical Pacific Ocean, and exerts influences on extratropical climate variability in both the Northern Hemisphere (NH) and Southern Hemisphere (SH) by atmospheric teleconnection (Philander et al., 1984; Zebiak and Cane, 1987; Mcphaden et al., 2006). Relationship between ENSO and the SH extratropical climate variations has been the focus of many studies, which have either revealed the ENSO induced anomalies of a specific climate variable such as the sea surface temperature (SST), the surface air temperature and the sea ice concentration (Turner, 2004; Gong et al., 2013; Li et al., 2013; Ciasto et al., 2015), or revealed the relations between ENSO and the dominant climate modes including the southern annular mode (SAM) and the Pacific-South America (PSA) wave train (Mo, 2000; Fogt and Bromwich, 2006; L'Heureux and Thompson, 2006; Fogt and Bromwich et al., 2011; Yu et al., 2015).

In the past decade, it was found that ENSO was transitioned from an eastern Pacific (EP) type to a central Pacific (CP) type in the late 1990s (Kao and Yu, 2009; Yu et al., 2011), with a transfer of the tropical SST anomaly center from the eastern to the central Pacific. Such transition has been documented to impose significant impacts on the SH extratropical climate variation patterns. Li et al. (2013) found that the two types of ENSO can stimulate different atmospheric circulation modes that further affect the SST variations in the South Pacific. Ciasto et al. (2015) suggested that in austral warm seasons, the EP SST variability is largely associated with zonally symmetric structures in the SH extratropical atmospheric circulation reflecting SAM and is strongly coupled with the SH SST and sea ice, while the CP ENSO has only weak impacts on the SH climate variables. Yu et al. (2015) was focused on the austral spring season, and concluded that a close relationship between SAM and ENSO was developed in this season when ENSO changed from the EP type to the CP type by both an eddy-mean flow interaction mechanism and a stratospheric pathway mechanism, and the CP ENSO type induced a stronger dipole structure in the sea ice concentration field in the Atlantic and Pacific sectors. Yeo and Kim (2015) investigated the decadal change in the SH SST associated with both ENSO and with SAM before and after 1999, and suggested a weakened ENSO teleconnection with the SH extratropics in austral autumn and winter. These previous studies have made great efforts in revealing the

Foundation item: The General Program of the National Natural Science Foundation of China under contract Nos 41876221 and 41861134040.

*Corresponding author, E-mail: zrzhang@sjtu.edu.cn

linkage between different types of ENSO and the SH extratropical climate patterns in different seasons, with most of them focused on specific variables like SST or on specific seasons. In this study, we attempted to uncover the linkage of the SH extratropical climate variability to the EP and CP ENSO over a full annual cycle for a variety of important climate variables including the atmospheric circulation, mixed layer temperature, mixed layer depth, air-sea heat fluxes and sea-ice concentration. In addition, in austral spring and summer, the seasons characterized by strong coupling between ENSO and the SH extratropical climate (Ciasto et al., 2015; Yu et al., 2015), the change in the ENSO-related anomalies of the climate variables mentioned above from the EP ENSO period to the CP ENSO period were associated with changes in the dominating climate modes in the SH extratropics.

2 Datasets and methods

2.1 *Dataset*

The reanalysis product used in this study is the Climate Forecast System Reanalysis (CFSR) covering the period 1979–2010 (Saha et al., 2010), which is produced by a coupled atmosphere-ocean-sea-ice system from the National Centers for Environmental Prediction (NCEP). CFSR uses the global forecast system (GFS) model as the atmospheric model. The ocean model is the Modular Ocean Model Version 4 (MOM4) that also includes a sea-ice module. This model has a zonal resolution of 0.5°, and a meridional resolution of 0.25° between 10°S and 10°N that increasing to 0.5° poleward of 30°S and 30°N. The model has 40 vertical layers. The sea-ice model grid is identical to the ocean model grid. CFSR assimilates sub-surface temperature and salinity observations from XBTs and the Argo array using a 3D-VAR scheme, and surface temperature and salinity from satellite and in-situ observations using an optimal interpolation scheme. Sea-ice concentration reanalysis data comes from the gridded data of Cavalieri (1994), the NCEP operational ice analysis, and a newer NCEP sea-ice analysis system (Saha et al., 2010). In this study, monthly data from CFSR were used to derive the climate indices and to analyze the relations of the SH extratropical atmospheric, oceanic and sea-ice processes to ENSO.

2.2 *Methods*

In this study, the CFSR dataset was separated into the period of 1979–1998 (hereafter 79–98) and the period 1999–2010 (hereafter 99–10), corresponding to the periods when ENSO is dominated by the EP type and the CP type, respectively. Variations of the EP and CP ENSO are characterized respectively by the Niño3 and Niño4 indices. The Niño3 index was obtained by calculating the anomalies of multi-year SST from CFSR over the eastern tropical Pacific (5°S–5°N, 90°–150°W), and the Niño4 index was obtained from the SST anomalies in the central tropical Pacific (5°S–5°N, 160°E–150°W). The SH extratropical area is defined as the region south of 20°S, and to study the relationship of the climate variables in this region to the ENSO variation, we first removed the long-term linear trend from the monthly timeseries data. Seasonal cycles were then removed from the detrended data to obtain the anomalies of the respective variables. The anomaly of a climate variable associated with the ENSO variation, which is defined as ERA (ENSO related anomaly) in this study, was then derived by performing a point-wise regression of the monthly anomaly timeseries of the respective variable to the Niño3 or Niño4 index depending on the period. The regression coefficient (slope), which denotes the anomaly of a variable corresponding to an one-standard-deviation increase in the Niño index, is then the ERA. Following Mo (2000) and Mo and Higgins (1998), indices of SAM, PSA1 and PSA2 were defined as the principle component time series associated with the first, second and third empirical orthogonal function (EOF) modes of monthly mean SLP data south of 20°S, respectively. Linear regression of SAM, PSA1 and PSA2 onto the ENSO indices were also performed to analyze the relationship between these climate modes for periods dominated by different ENSO types. The ENSO relate climate variable variations are examined in different seasons, and in this study the austral summer, autumn, winter and spring were denoted by DJF (December, January and February), MAM (March, April and May), JJA (June, July and August) and SON (September, October and November) respectively.

3 Results and discussion

3.1 *Variations of the SH extratropic atmospheric variations associated with the EP and CP ENSO*

3.1.1 *Sea level pressure*

Figure 1 shows the spatial distributions of the SH extratropical SLP ERAs related to the Niño3 or Niño4 variations for the 79–98 and 99–10 periods and in the four seasons. Significant SLP anomalies related to the Niño3 or Niño4 changes are observed in all of the four seasons, while the coupling between ENSO and SLP at high latitudes (south of 60°S) are stronger in spring and summer, which is consistent with previous studies (e.g., Fogt and Bromwich, 2006). In spring, the SLP ERA fields related to Niño3 and to Niño4 in 79–98 are similar (Figs 1d , h), and they are both characterized by two negative anomaly centers in the western Atlantic sector and the western Pacific sector, and a positive anomaly center in the eastern Pacific sector. This pattern resembles the distribution of a negative phase of PSA2. The coefficient of correlation between Niño3 and the PSA2 index is –0.59, and the coefficient of correlation between Niño4 and the PSA2 index is –0.53 (Table 1). These correlations are both significant at the confidence level of 95%. In the period 99–10 (Figs 1l , p), however, the SLP ERA field bears no resemblance to PSA2. Instead, the SLP ERA field shows a dipole structure with a positive anomaly center in the Amundsen Sea and Ross Sea, and a negative anomaly center east of New Zealand. Such structure shows similarity to the pattern of a positive phase of SAM in the Pacific sector (Zhang et al., 2018), and the correlation coefficients between Niño3 and SAM and between Niño4 and SAM are –0.33 and –0.42, respectively, which are respectively significant at the confidence level of 95% and 90%. These results support the finding from Yu et al. (2015) that there is strong relationship between SAM and ENSO when ENSO was transitioned into a CP type in the 1990s. On the other hand, a significant relationship between PSA1 and Niño3 (Table 1) in 79–98 does not appear in 99–10, which is consistent with the results from Yeo and Kim (2015) that the Rossby wave response to anomalous Equatorial heating/cooling is weaker in the CP ENSO period.

In the summer of 1979–1998 (Figs 1a ,e), the positive anomaly center in the eastern Pacific sector is still noticeable, while the negative centers in the Atlantic sector and the western Pacific sector are much weaker compared to those in spring. The SLP ERA fields exhibit a PSA-like pattern in the Pacific sector, with alternative signs from the mid to high latitudes depicting a wave train. The PSA1 index is neither significantly correlated with Niño3 nor Niño4 (Table 1), while the correlation coefficients between Niño3 and PSA2 and between Niño4 and PSA2 still reach –0.55 and –0.57 respectively, both of which are significant

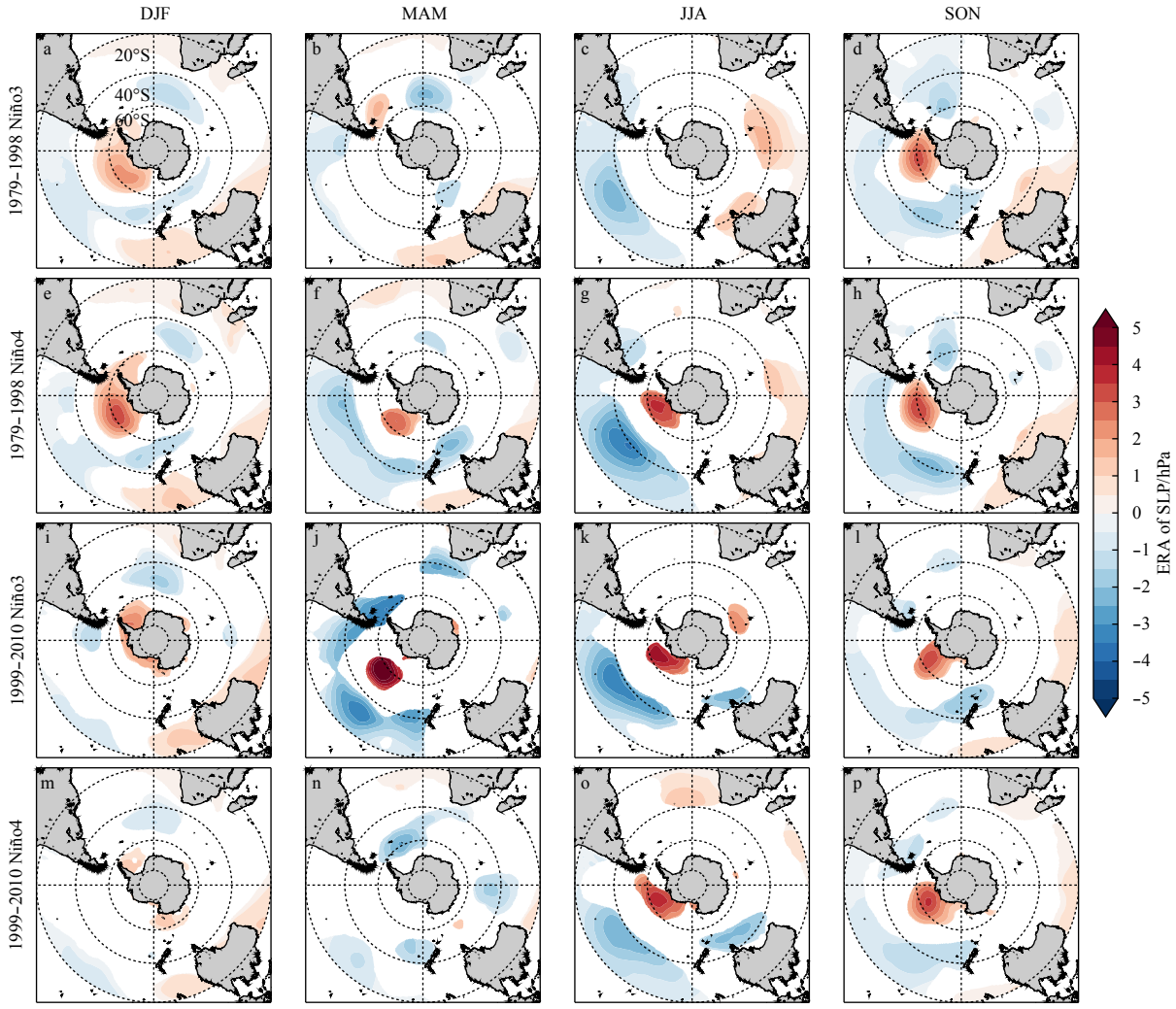

Fig. 1. Spatial distributions of the ERAs of SLP associated with the Niño3 or Niño4 variations for 1979–1998 (a–h) and for 1999–2010 (i–p) during austral (first column) summer, (second column) autumn, (third column) winter and (fourth column) spring seasons. Only areas where the ERAs are statistically significant at the 90% confidence level are shaded.

Table 1. Coefficients of correlation between the Niño3 Index or Niño4 Index and the SAM, PSA1, and PSA2 Indices in 1979–1998 and 1999–2010 in the four seasons

Indices	1979–1998				1999–2010			
	DJF	MAM	JJA	SON	DJF	MAM	JJA	SON
Niño3–SAM	**–0.29***	0.01	0.03	–0.18	**–0.31**	–0.24	–0.18	**–0.33***
Niño3–PSA1	0.07	–0.20	–0.21	**0.27**	0.23	0.22	0.16	–0.07
Niño3–PSA2	**–0.55***	–0.10	–0.28	**–0.59***	0.28	**–0.37**	**–0.28**	–0.18
Niño4–SAM	**–0.24**	–0.12	–0.16	–0.11	–0.26	–0.27	–0.23	**–0.42***
Niño4–PSA1	0.03	–0.11	**–0.23**	–0.01	0.19	0.21	0.16	–0.03
Niño4–PSA2	**–0.57***	**–0.31***	**–0.20**	**–0.53***	0.17	0.01	**–0.28**	–0.23

Note: Bold numbers denote correlations significant at the 90% confidence level, and numbers with stars denote correlations significant at the 95% confidence level.

at the 95% confidence level. The coefficients of correlations between Niño3 and SAM and between Niño4 and SAM are –0.29 and –0.24 respectively, which are also respectively significant at the 95% and the 90% confidence level. For the summer of 99–10 (Figs 1i , m), a PSA-like pattern nearly disappears in the SLP ERA field, and neither the correlation between Niño3 and PSA2 nor between Niño4 and PSA2 is significant. The decadal variability in the ENSO-PSA2 relationship over the two periods are similar to that in spring. On the other hand, the correlation between Niño3 and SAM is –0.31 and is significant at the 90% confidence level, while that between Niño4 and SAM is not statistically significant. Ciasto et al. (2015) found that during the austral warm season, the EP SST variability is correlated with SAM and the CP SST variability exhibits no clear association with SAM. Our results indicate that in summer significant relationships exist both between SAM and the EP SST variability and between SAM and the CP SST variability during the EP ENSO period, while the association of SAM with the CP SST variability is broken down during the CP

ENSO period.

Significant SLP ERAs associated with Niño4 and Niño3 are also observed in the autumn and winter of 79–98 (Figs 1f , g) and of 99–10 (Figs 1g , k), respectively. The ERA patterns show resemblance to those in spring, while the positive anomalies are mostly confined south of 60°S in the Amundsen Sea and eastern Ross Sea. For these two seasons, correlations between Niño4 and PSA2 during 79–98 and between Niño3 and PSA2 during 99–10 are both significant at the 90% confidence level, and for both periods the correlation coefficients for autumn are higher than those for winter. For autumn and winter, no significant correlations are found either between Niño3 and SAM or between Niño4 and SAM for either of the two periods. While PSA1 is also one of the dominant modes for the SH extratropical climate variability, we see in Fig. 1 that prominent PSA1-like signatures only appear in the SLP ERA field in the summer of 79–98, while statistically significant correlation between ENSO and PSA1 is only found in the winter season of 79–98 between Niño4 and PSA1 and the spring season of 79–98 between Niño3 and PSA1, with low correlation coefficients below 0.3. Therefore the results from this study suggest that PSA2 plays a more important role in the linkage of the SH subtropical climate variability to ENSO.

Comparing all the SLP ERA fields in Fig.1, it is noted the weakest SLP anomalies occur in the summer of 99–10 related to Niño4, the autumn of 79–98 related to Niño3, the autumn of 99–10 related to Niño4 and the winter of 79–98 related to Niño3, corresponding to the four periods without any significant correlations of ENSO to either of the major climate modes dominating the SH extratropical climate variability, i.e., SAM, PSA1 or PSA2 (Table 1). On the other hand, comparing the SLP ERA fields associated either with Niño3 or with Niño4 between the 79–98 and 99–10 periods, we cannot reach a conclusion that the ERAs induced by Niño3 variations are stronger in 79–98 when ENSO is dominated by the EP type, and that ERAs induced by Niño4 variations are stronger in 99–10 when ENSO is dominated by the CP type. In fact, in the EP ENSO period 79–98, during spring and summer the SLP ERAs induced by Niño3 and Niño4 variations are comparable, while during autumn and winter the SLP ERAs related to Niño4 are even stronger than those related to Niño3. In the CP ENSO period, during spring and winter there are no considerable differences between the SLP ERAs related to Niño3 and the ERAs related to Niño4, while during summer and spring the SLP anomalies related to Niño3 are even stronger than those related to Niño4. These indicate that the SH extratropical atmo-

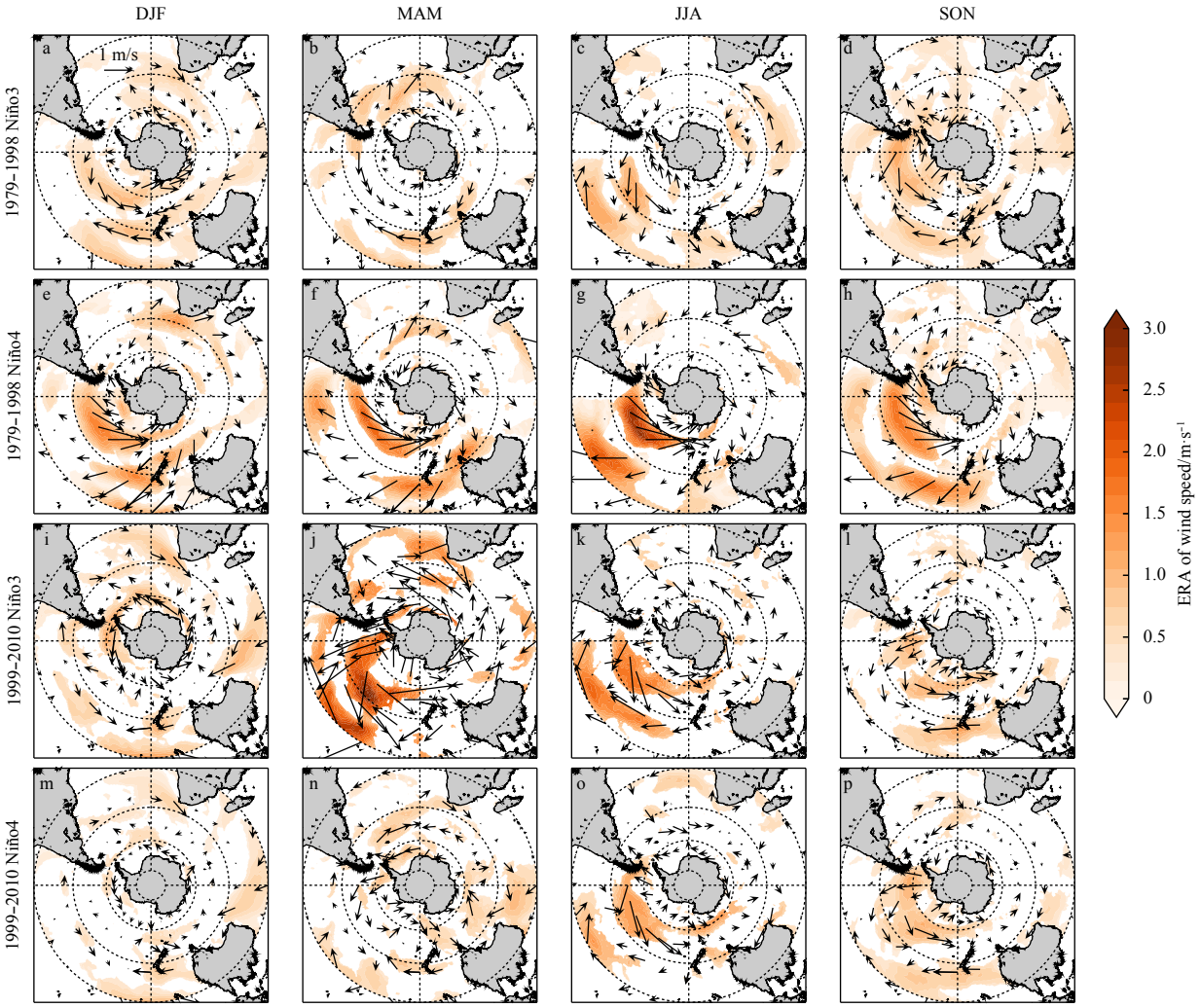

Fig. 2. Spatial distributions of the ERAs of 10-m wind vector (arrow) and wind speed (color) associated with the Niño3 or Niño4 variations for 1979–1998 (a–h) and for 1999–2010 (i–p) during austral (first column) summer, (second column) autumn, (third column) winter and (fourth column) spring seasons. Only areas where the ERAs are statistically significant at the 90% confidence level are shaded.

spheric variations associated with a specific ENSO type are not necessarily strong when this ENSO type is dominant.

3.1.2 *Surface wind*

Figure 2 shows the ERAs fields of the SH extratropical surface (2 m) wind related to the Niño3 or Niño4 variations for the 79–98 and 99–10 periods. The surface wind ERA distributions show a close correspondence to the SLP ERA distributions, such that a positive (negative) anomaly center in the SLP field is generally accompanied by anticyclonic (cyclonic) wind anomalies. In spring, the wind ERA field is generally characterized by westerly wind anomalies in the mid latitudes and easterly wind anomalies in the high latitudes, while noticeable anticyclonic wind anomalies are observed in the central and eastern Pacific sector corresponding to the positive SLP anomaly center (Fig. 1). It is noted that in the spring of 79–98, while the SLP anomaly field associated with Niño4 (Fig. 1h) is similar to that with Niño3 (Fig. 1d), the wind anomaly field shows noticeable differences. The anticyclonic anomaly structure in the central and eastern Pacific sector associated with Niño4 is weaker compared to those associated with Niño3, and instead it is mainly characterized by northeast wind anomalies on the northern branch of the anticyclone. The northeasterly anomalies, instead of southeasterly anomalies in the same region as in Fig. 1d, are a result of a weakened correlation between ENSO and PSA2 that results in weak SLP anomalies in the western Pacific sector between 40°S and 60°S. The difference between the ERA field associated with Niño3 and that associated with Niño4 in 79–98 also occurs in the summer, autumn and winter seasons in the same period (Figs 1e–g). In 99–10, no significant differences are observed between the wind ERA field associated with Niño3 and that associated with Niño4 in winter and spring, while in autumn the wind ERAs associated with Niño3 are strongest among all of the wind ERA fields, correlated with strong SLP ERAs. This is the period when the ENSO variation is only significantly correlated with PSA2, and the fact that there is no influence from the other major climate modes such as SAM and PSA1, and thus no offset in the climate variable anomalies may result in the strong SLP ERAs in this period. For the surface wind, same as SLP, there is no evidence that the ERAs induced by Niño3 variations are stronger in the EP ENSO dominated period, and that ERAs induced by Niño4 variations are stronger in the CP ENSO dominated period.

3.1.3 *Surface air temperature (SAT)*

Figure 3 shows the ERAs fields of the SH extratropical SAT related to the Niño3 or Niño4 variations for the 79–98 and 99–10

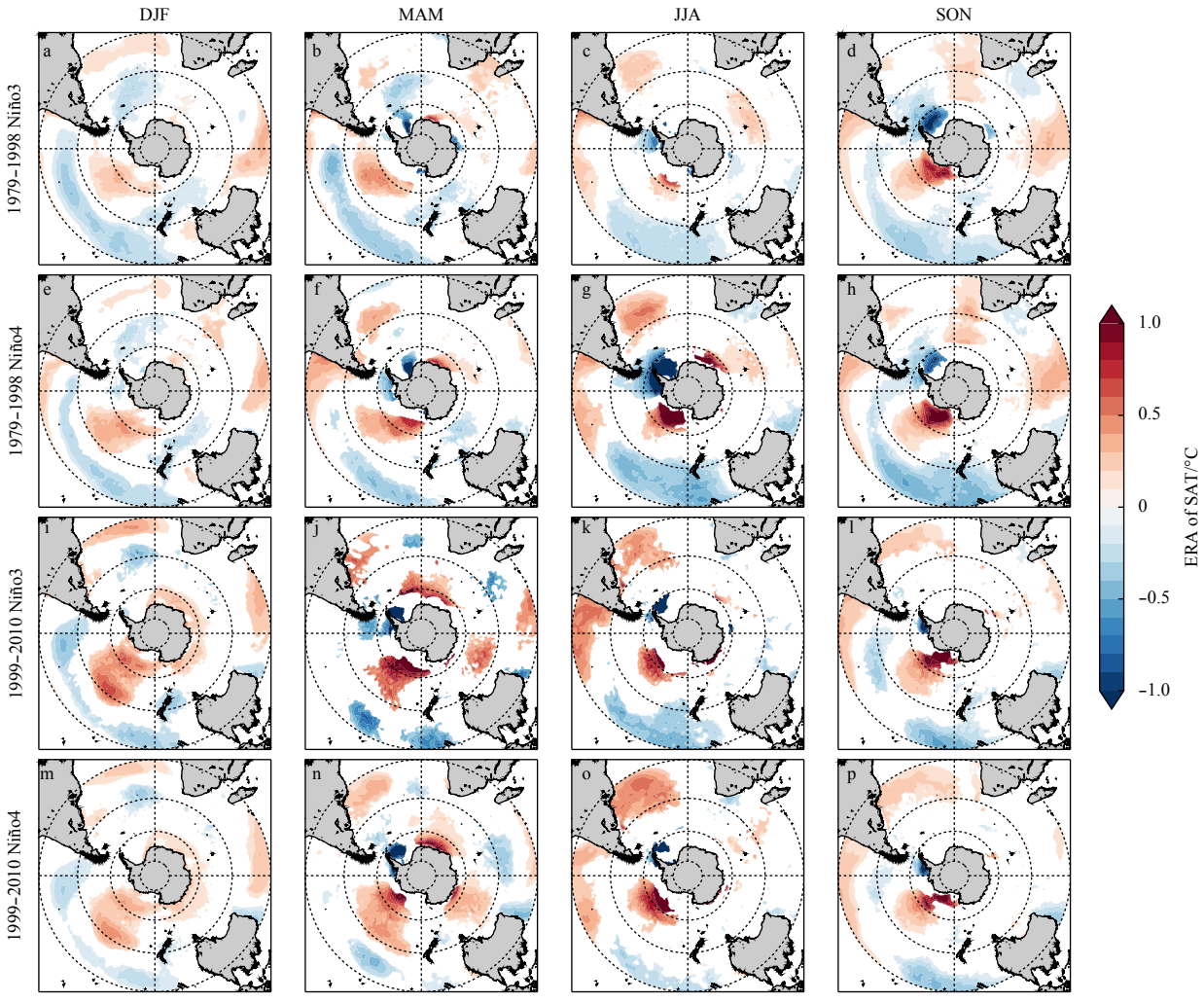

Fig. 3. Spatial distributions of the ERAs of SAT associated with the Niño3 or Niño4 variations for 1979–1998 (a–h) and for 1999–2010 (i–p) during austral (first column) summer, (second column) autumn, (third column) winter and (fourth column) spring seasons. Only areas where the ERAs are statistically significant at the 90% confidence level are shaded.

periods. The SAT anomalies are largely determined by the surface wind anomalies. For example, in the regions dominated by anticyclonic wind anomalies, such as in the central and eastern Pacific sector in most subplots of Fig. 3, the SAT anomaly field is characterized by a negative center near the Antarctic Peninsula and a positive center in the central Pacific sector, which are respectively created by the southward advection of warm air from the lower latitudes and northward advection of cold air from the Antarctic continent by the anomalous anticyclone. In the spring of 79–98, the period when a strong relation exists between PSA2 and ENSO (Table 1), SAT exhibits the strongest ERAs associated with both of Niño3 or Niño4 in the high latitudes, and particularly in the eastern Pacific sector and the western Atlantic sector as for the SLP ERAs. Associated with the prominent negative SLP anomaly center in the western Atlantic sector in the spring of 79–98 (Figs 1d, h) and the related anomalous cyclonic winds (Figs 2d , h), which appear as a result of the strong coupling between PSA2 and ENSO, the SAT anomaly field in the Atlantic sector exhibits a dipole structure with strong negative SAT anomalies east of the Antarctic Peninsula and noticeable positive SAT anomalies in the eastern Atlantic sector. Such anomalies patterns are found to exert significant impacts on the anomaly field of the mixed layer temperature and sea ice concentration, as will be discussed below. Strong SAT anomalies also occur in the winter of 79–98 associated with Niño4 (Fig. 3g), the only season in which significant correlation between ENSO and PSA1 exists (Table 1). Another notable feature in the SAT ERA field is that in the autumn of 99–10 (Figs 3j , n), the anomaly patters are both dominated by three positive centers in the mid latitudes, indicating a wavenumber-3 structure. For the anomaly field associated with Niño3 (Fig. 3j), this structure can be explained by the close relation between Niño3 and PSA2 in this season as shown in Table 1, while for the anomaly field associated with Niño4, there are no significant correlations of Niño4 either with PSA2, PSA1 or SAM. The SLP and surface wind ERAs are also quite weak in this season, implying that the SAT anomalies are not resulted from the wind anomalies but instead from other processes. It is noted that significant anomalies associated with Niño4 are found for the mixed layer temperature (MLT) in the autumn of 99–10 (Fig. 4n) and are characterized by a wavenumber-3 structure in the mid and high latitudes, with three positive anomaly centers located exactly in the same regions as the SAT positive anomaly centers, seemingly capable of explaining the SAT anomaly pattern through a oceanic feedback to the atmosphere. However, the surface heat flux anomalies at the three positive SAT anomaly centers are positive (Fig. 5n), meaning that the net heat fluxes are

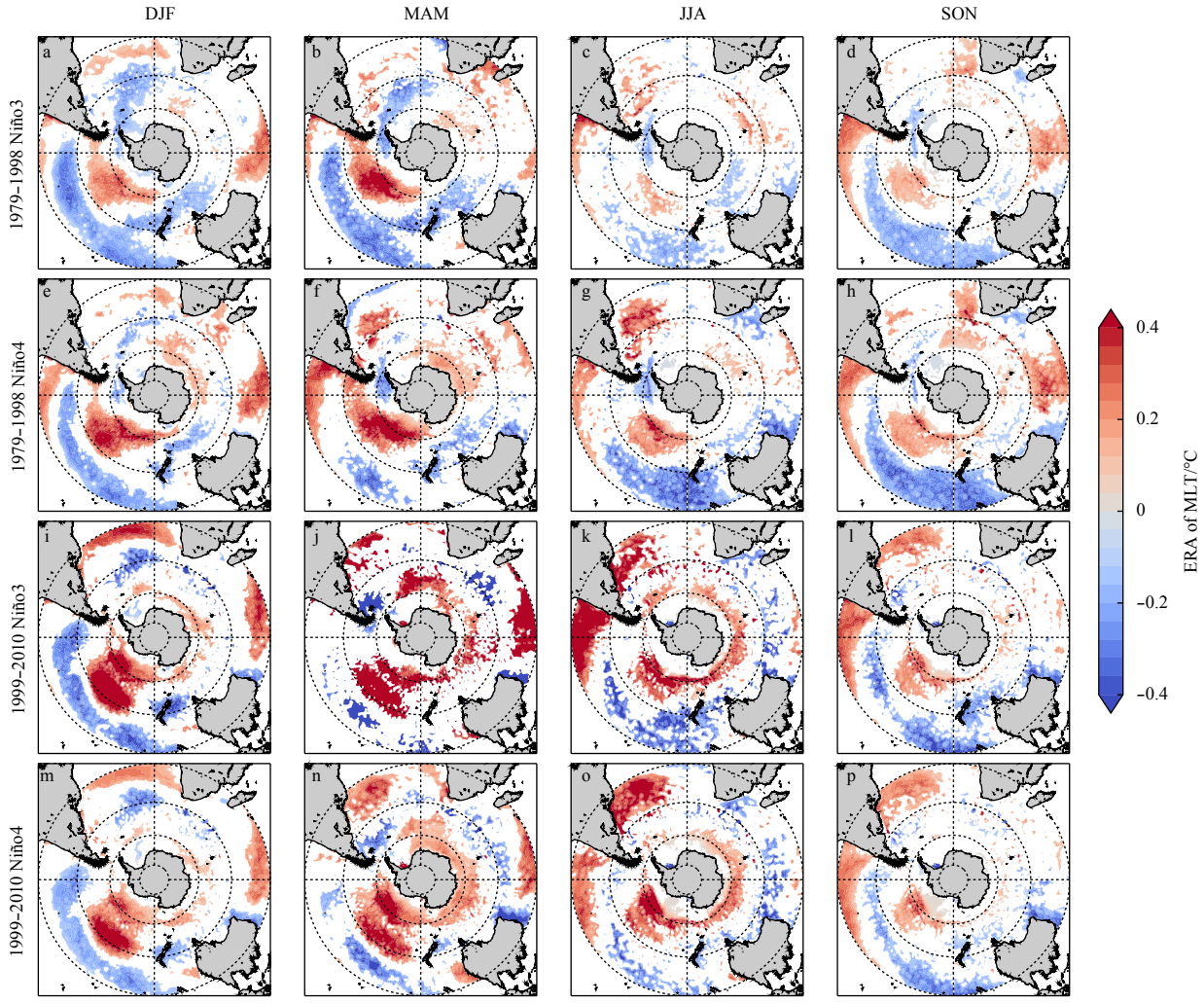

Fig. 4. Spatial distributions of the ERAs of MLT associated with the Niño3 or Niño4 variations for 1979–1998 (a–h) and for1999–2010 (i–p) during austral (first column) summer, (second column) autumn, (third column) winter and (fourth column) spring seasons. Only areas where the ERAs are statistically significant at the 90% confidence level are shaded.

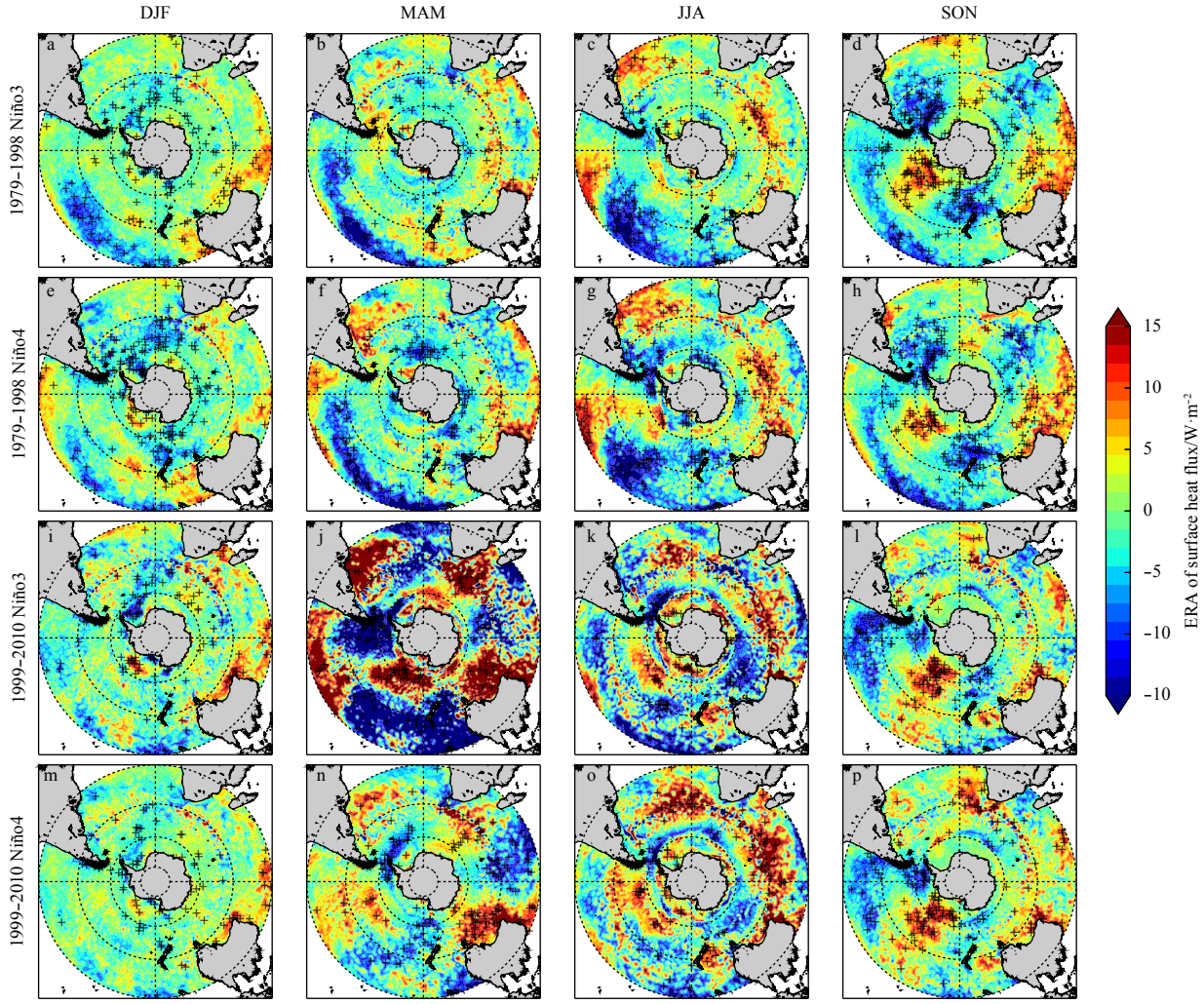

Fig. 5. Spatial distributions of the ERAs of total surface heat flux associated with the Niño3 or Niño4 variations for 1979–1998 (a–h) and for 1999–2010 (i–p) during austral (first column) summer, (second column) autumn, (third column) winter and (fourth column) spring seasons. Only areas where the ERAs are statistically significant at the 90% confidence level are shaded.

from the atmosphere into the ocean and that it is the SAT anomalies modulating the MLT anomalies rather than the other way round. Therefore the SAT anomalies are created by anomalies of other atmospheric processes, and probably by cloudiness that is not included in this study.

On the other hand, significant positive SAT anomalies are observed in the autumn of 1979–1998 associated with Niño3 in the central Pacific sector (Fig. 3b), while the SLP and surface wind anomalies are quite weak and insignificant (Figs 1b, 2b). The strong positive anomalies in the MLT field (Fig. 4b) together with the weak, but significant negative anomalies in the total surface heat flux field (Fig. 5b) in this region suggest that the positive SAT anomalies are modulated by the positive MLT anomalies by the ocean-to-atmosphere heat fluxes. It is unknown that if the MLT anomalies are directly affected by the ENSO variations via an ocean teleconnection or affected by atmospheric variables like clouds or precipitation via an atmosphere teleconnection and then atmosphere-ocean interaction. As shown in Table 1, in the autumn of 79–98 there is no significant correlation of the Niño3 index to either of the dominant SH climate variation indices, i.e. SAM, PSA1 or PSA2. Therefore, it is very likely that the MLT anomalies are resulted from ocean teleconnection, the mechanism behind which demands further analysis that is beyond the scope of this study.

3.2 *Variations of the SH extratropical oceanic variations associated with the EP and CP ENSO*

3.2.1 *Mixed layer temperature*

As mentioned above, in most cases the MLT ERA field shows a resemblance to the SAT ERA field by the atmosphere-ocean interactions, such that positive (negative) anomaly centers of SAT are normally followed by positive (negative) anomaly centers of MLT by atmosphere-ocean heat fluxes. A positive anomaly center in the central Pacific sector is a persistent feature in the MLT ERA field in both periods and in all seasons resembling the SAT anomaly pattern. A major difference from the SAT anomaly field is that the positive MLT anomaly centers in the central Pacific sector are strongest in summer and autumn, and weakest in spring when the SAT anomalies are quite strong. The decoupling between the MLT and SAT anomalies in spring are associated with the surface wind anomalies, which have a strong northward component in the eastern Pacific sector (the eastern branch of the anomalous cyclone) that transports cold water near Antarc-

tica to the central Pacific area by Ekman flows, which are directed leftward of the anomalous winds. Therefore, the MLT anomalies are co-influenced by the SAT anomalies via air-sea heat fluxes and by surface wind anomalies via advective oceanic heat fluxes.

In the spring of 79–98 that is characterized by significant correlation between PSA2 and ENSO, similar to the SAT anomaly pattern, a dipole structure appears in the MLT anomaly field in the Atlantic sector, with significant negative anomalies near the Antarctic Peninsula and positive anomalies in the eastern Atlantic sector. This dipole structure is absent in the spring of 99–10. Such decadal variation reflects the variation in the surface heat flux anomaly field in spring (Figs 5d–h): large-scale negative and positive heat flux anomalies exist in the western and eastern Atlantic sectors respectively in 79–98, which nearly disappear in 99–10. Significant decadal variations in the MLT anomaly field also exist in autumn when the negative anomalies in the western Antarctic Peninsula region and in the western Pacific sector in 79–98 disappear in 99–10, and in winter when the MLT anomaly field turns into a more annular structure in 99–10. While there are no significant correlations between SAM and Niño3 or between SAM and Niño4 in the winter of 99–10 (Table 1), the wind anomaly fields do exhibit an annular structure in this period (Figs 2k, o), which are responsible for the annular patterns in the MLT anomaly fields by advective heat fluxes associated with wind-driven Ekman transports. Yeo and Kim (2015) observed a prevailing of warm SST anomalies in the Pacific sector east of New Zealand in spring and summer when CP ENSO dominates, which is associated with a westward shift of positive SLP anomalies in the Pacific. Such phenomenon is not observed in the MLT anomaly fields in Fig. 3, though weak negative MLT anomalies east of New Zealand in 79–98 become obscure in 99–10.

3.2.2 *Mixed layer depth (MLD)*

The MLD ERA field shows a good correspondence to the surface heat flux and MLT ERA fields with an anti-correlation, consistent with the results from Sallee et al. (2010) and Zhang et al. (2018) that the SH extratropical MLD anomalies are majorly controlled by the surface heat flux anomalies. Occasionally, surface wind also plays a significant role in the MLD anomalies. In the spring of 79–98, the heat flux ERA fields associated with both Niño3 and Niño4 show prominent signatures of PSA2 and are dominated by a zonal wavenumber-3 structure in the mid and high latitudes (Figs 5d,h). The MLD anomaly field is featured by a positive center in the western Atlantic sector and a negative center in the eastern Pacific sector, collocated with the negative and

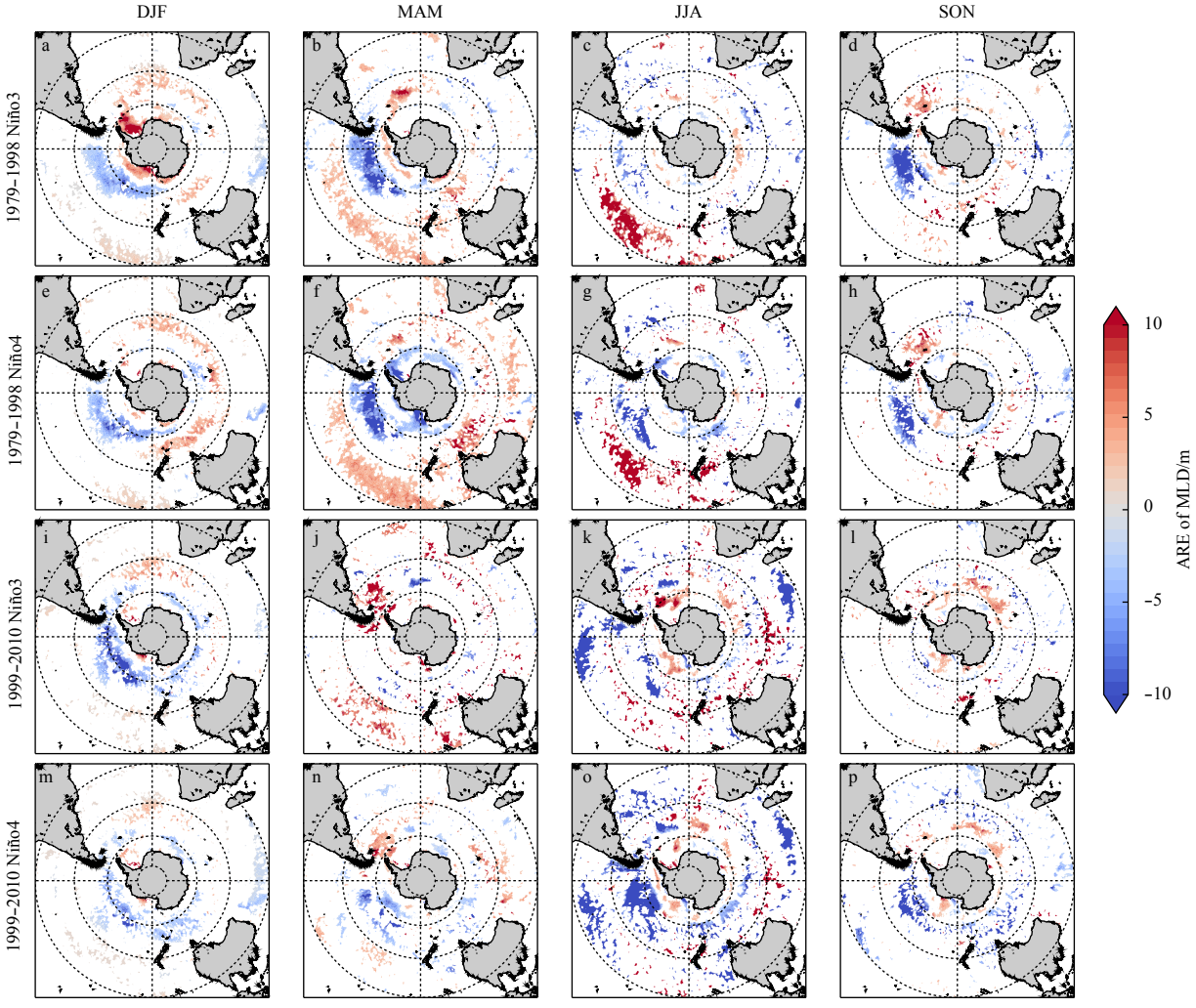

Fig. 6. Spatial distributions of the ERAs of MLD associated with the Niño3 or Niño4 variations for 1979–1998 (a–h) and for 1999–2010 (i–p) during austral (first column) summer, (second column) autumn, (third column) winter and (fourth column) spring seasons. Only areas where the ERAs are statistically significant at the 90% confidence level are shaded.

positive heat flux anomaly centers respectively. The absence of significant MLD anomalies in the western Pacific sector where significant heat flux anomalies exist is a result of weak, insignificant wind anomalies. The dipole structure in the MLD anomaly field disappears in the autumn of 99–10 (Figs 6l , p) when a close ENSO-PSA2 relation no longer exists. Significant decadal variations in the ERA field of MLD are also found for the autumn season, when strong negative MLD anomalies south of 40°S in the eastern Pacific sector and positive anomalies across the Pacific sector between 40°S and 20°S associated with strong negative heat flux anomalies become hardly detectable in 99–10. The latter is associated with the disappearance of the elongated surface heat flux anomalies in the mid latitudes of the Pacific Ocean in 99–10, while the former is a result of disappeared positive MLT anomalies in the eastern Pacific sector in conjunction with nil easterly wind anomalies (which will not weaken the prevailing westerlies and thus will not result in shallowed MLD) in this area.

It is also noted that while the heat flux anomalies in Fig. 5j are strongest among all of the heat flux ERA fields, which results from the strongest surface wind anomalies existing in the same period (Fig. 2j), the respective MLD anomalies (Fig. 6j) as well as the MLT anomalies (Fig. 4j) are quite weak. Besides winds and surface heat fluxes, advection and vertical mixing are the other two factors that play a significant role in the MLD variation (Sen Gupta and England, 2006). It is very likely that the strong wind anomalies have led to strong anomalous horizonal advection of heat that could cancel out the heat anomalies brought by the atmosphere-ocean heat exchange. One possible evidence for such hypothesis is that in the central Pacific sector, which is characterized by strong positive heat flux anomalies (Fig. 5j) but weak MLD and MLT anomalies (Figs 6j and 7j). This could result from the fact that the strong anomalous anticyclonic wind in this area induces westward Ekman transport on its eastern branch and eastward Ekman transport on its western branch, carrying waters from the negative MLT anomaly centers in the eastern and western Pacific sector to the positive MLT anomaly center in central Pacific and thus resulting ultimately in weak MLT and MLD anomalies in this region.

3.3 *Variations of the SH extratropical sea-ice variations associated with the EP and CP ENSO*

Finally, we examined the spatial distributions of the SH extratropical sea-ice concentration (SIC) ERAs related to the Niño3 or Niño4 variations during the EP-ENSO dominated period and the CP-ENSO dominated period. The SIC anomaly patterns are examined only in austral spring, i.e. the season when ice extent reaches the maximum in the southern hemisphere. In both periods and related to both of the Niño3 and Niño4 variations, there are positive SIC anomalies near the Antarctic Peninsula and negative SIC anomalies in the central Pacific sector between 60°S

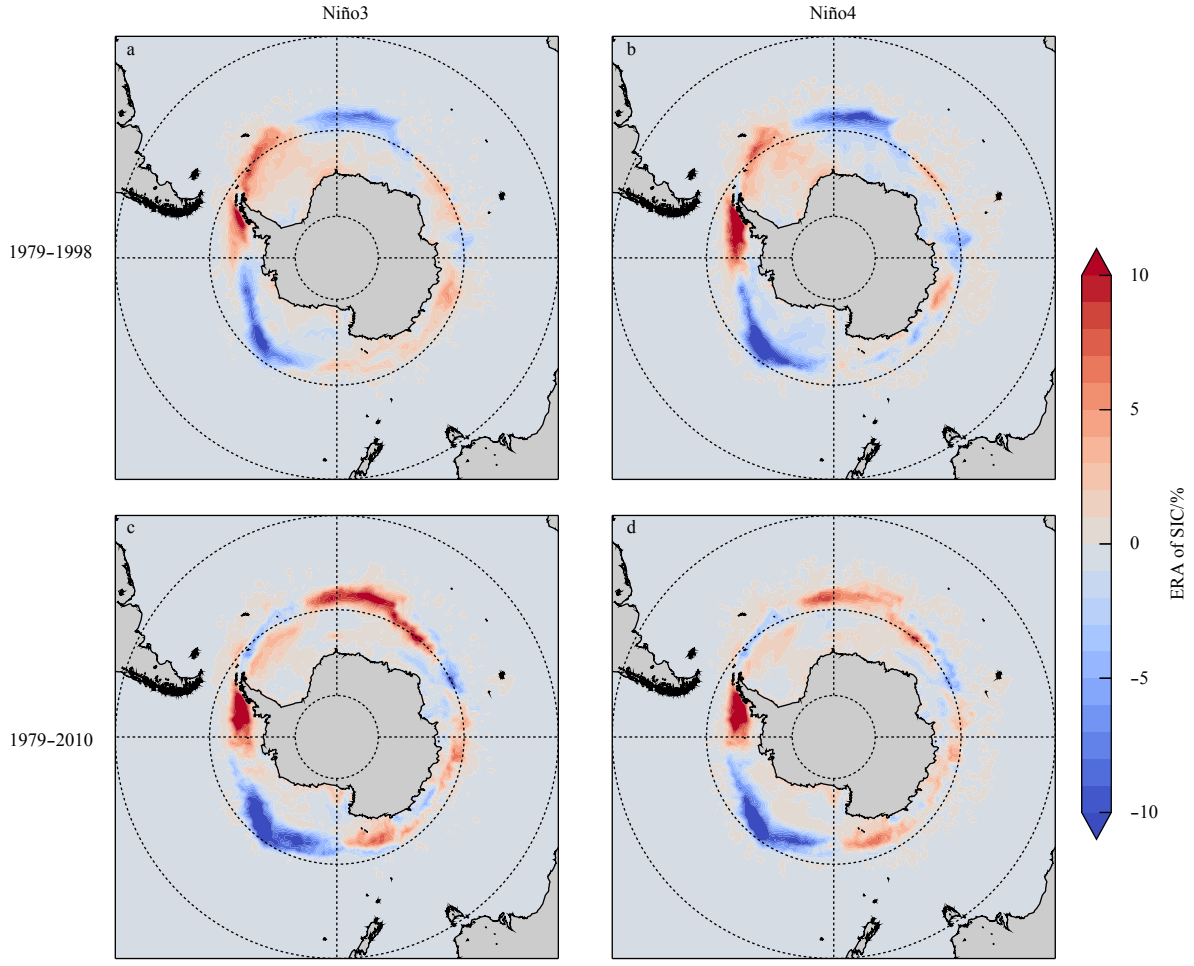

Fig. 7. Spatial distributions of the ERAs of sea-ice concentration associated with the Niño3 or Niño4 variations for 1979–1998 (a , b) and for 1999–2010 (c , d) during austral spring. Only the areas where the ERAs are statistically significant at the 90% confidence level are shaded.

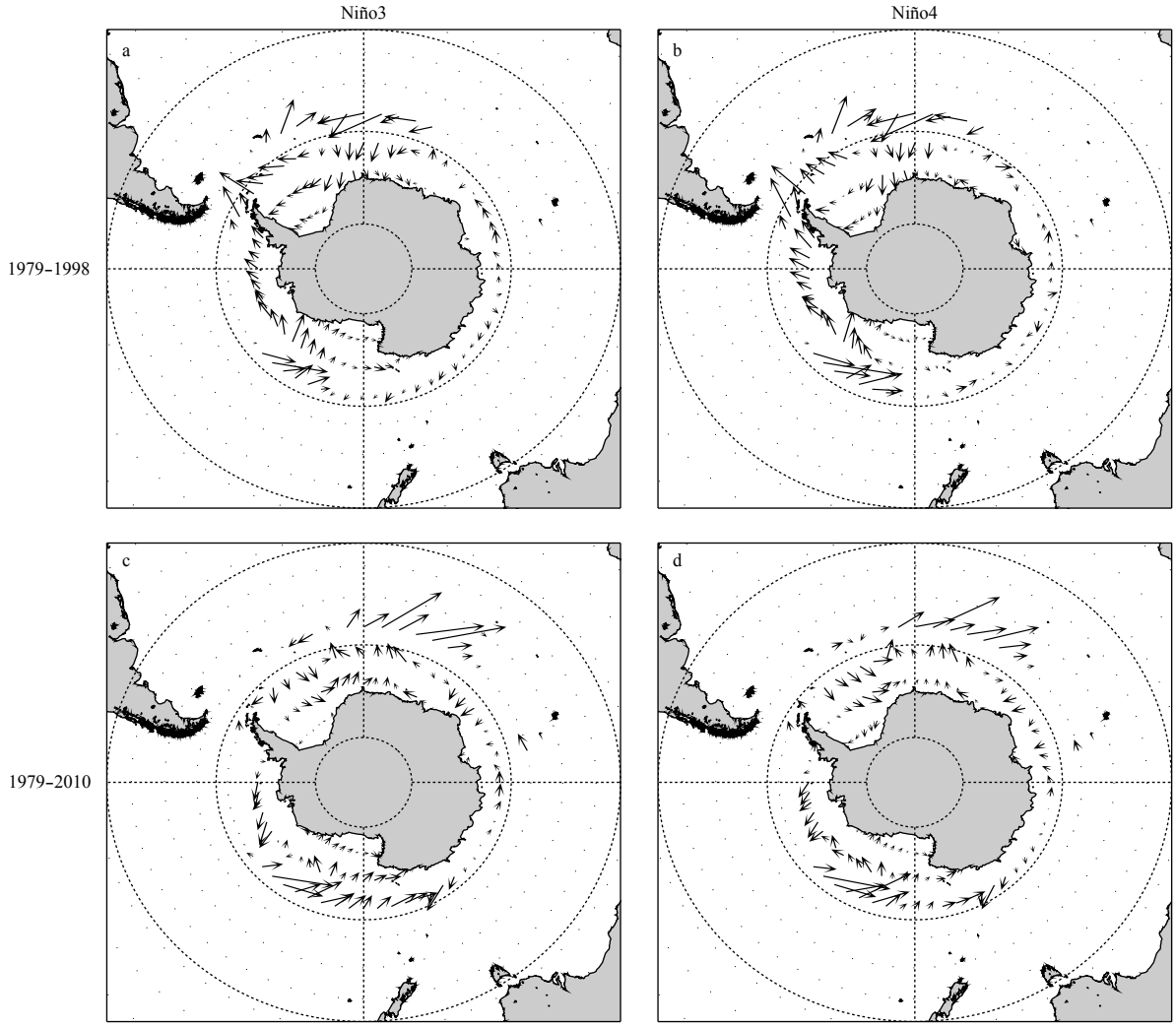

Fig. 8. Spatial distributions of the ERAs of the sea-ice velocity associated with the Niño3 or Niño4 variations for 1979–1998 (a , b) and for 1999–2010 (c , d) during austral spring.

and 65°S, corresponding to the positive and negative SAT anomalies in the respective regions. One of the major differences between the 79–98 period and the 99–10 period occurs in the eastern Atlantic sector, where the negative SIC anomalies in 79–98 change to positive anomalies in 99–10. This is associated with the disappearance of positive anomalies of SAT and MLT in the eastern Atlantic sector during the transition from the EP ENSO to the CP ENSO, which is in turn related to the disappearance of a close relation between ENSO and PSA2 during the transition. To investigate why positive SIC anomalies appear in the eastern Atlantic sector in the 99–10 period, we analyzed the corresponding ERA field of the sea-ice velocity as shown in Fig. 8. It is noticed that in 79–98, the sea-ice drift anomaly field is dominated by divergence in the area where SIC anomalies show significant decadal variability before and after 1999 (55°–60°S, 20°W–30°E; Figs 8a, b), while in 99–10, noticeable convergence patterns appear and begin to dominate the above area near 60°S. Such convergence is created by the convergence in the anomalous wind field in this region (Figs 2l ,p) and results in the positive SIC anomalies mentioned above. Another notable difference in the SIC ERA fields exists in the east of the Antarctic Peninsula around 60°S, where significant positive SIC anomalies in 79–98 change to slightly negative values in 99–10. This is also associated with the decoupling of PSA2 to ENSO in the CP ENSO period, when the negative SAT and MLT anomalies found in 79–98 in this area are obscure in 99–10. Ciasto et al. (2015) observed that in both of the austral cold season (June through September) and the warm season (November through February), compared to the EP-ENSO related SIC anomalies, the CP-ENSO related anomalies exhibit more negative values in the Eastern Hemisphere between 90°E and 180°E associated with a westward displacement of anticyclonic atmospheric circulation. Such feature is not observed in the SIC ERA field in the spring season of our study, as Fig. 7 shows that the SIC anomalies between 90°E and 180°E are even more positive in the CP ENSO period relative to the EP ENSO period.

4 Conclusions

Based on the CFSR reanalysis dataset that is produced by a coupled atmosphere-ocean-sea-ice system, this study investigated the variations of the Southern Hemisphere extratropical climate variables to the ENSO variations during two periods that are respectively dominated by the EP type ENSO and the CP type ENSO. In particular, we analyzed the ENSO related climate anomalies over an annual cycle. The relations of the SH extratropical climate variables to ENSO are examined by the anomalies of the variables related to an one-standard-deviation increase in the Niño3 or Niño4 index. It is found that during austral spring,

which is considered as the season with the strongest coupling between the SH extratropical climate and the tropics, the differences in the ENSO-related SLP anomaly patterns between the EP ENSO period (1979–1998) and the CP ENSO period (1999–2010), which are most notable in the Pacific sector, are primarily linked to the relationship between ENSO and PSA2 in 1979–1998, which is significant in the EP ENSO period and obscure in the CP ENSO period. A significant correlation is built up between SAM and ENSO during the CP ENSO period. The difference in the ENSO-PSA relationship affects the ENSO-related anomaly fields of surface wind, surface air temperature, mixed layer temperature and finally the Southern Ocean sea-ice concentration in spring. In austral summer, the decadal variability in the ENSO-PSA2 relationship from the EP ENSO period to the CP ENSO period is similar to that in spring. In addition, in 1979–1998 significant correlation exists between the variations of SAM and both of the variations of Niño3 and Niño4, while in 1999–2010 the correlation between SAM and Niño4 disappears. There are no significant correlations found between either of the major climate modes dominating the SH extratropics (SAM, PSA1 and PSA2) to Niño4 in the summer and autumn of 1999–2010, or to Niño3 in the autumn and winter of 1979–1998, resulting in the weakest ENSO-related anomalies in the sea level pressure field. There is no evidence that the SH extratropical climate variability induced by Niño3 variations are stronger in 1979–1998 when ENSO is dominated by the EP type, and that variability induced by Niño4 variations are stronger in 1999–2010 when ENSO is dominated by the CP type.

The surface air temperature anomaly patterns are basically controlled by the surface wind anomalies, which are further mirrored by the mixed layer temperature anomalies by atmosphere-ocean heat fluxes. There are occasionally situations that the SAT anomalies do not follow those of winds, which are inferred to be affected by the anomalies of other atmospheric processes like cloudiness and oceanic processes through ocean-to-atmospheric heat fluxes. The mixed layer depth anomalies are generally anti-correlated with the anomalies of surface heat fluxes and mixed layer temperature, while the role of wind occasionally overwhelms that of the heat fluxes in determining the MLD anomaly patterns. There are strikingly strong anomalies of surface heat fluxes resulting from strong surface wind anomalies in the autumn of 1979–1998 related to the Niño3 variation, the period when there is only significant correlation between ENSO and PSA2, but such extremely strong heat flux anomalies seem not transitioned into the mixed layer temperature and mixed layer depth anomalies. Considerable differences exist in the sea-ice concentration anomaly field between the 1979–1998 and the 1999–2010 periods, with negative and positive SIC anomalies in the eastern and western Atlantic sector in the former period replaced respectively by positive and weak negative anomalies in the latter period. Such change is found to be associated with the change in the anomaly fields of air temperature and mixed layer temperature, which are in turn linked to the change in the ENSO-PSA2 correlation.

Acknowledgements

The Climate Forecast System Reanalysis (CFSR) were obtained from the National Centers for Environmental Prediction (NCEP) and are available at https://rda.ucar.edu/datasets/ds093.2/. We thank the anonymous reviewers for their fruitful comments on improving this manuscript.

References

Ciasto L M, Simpkins G, England M H. 2015. Teleconnections between Tropical Pacific SST anomalies and extratropical southern hemisphere climate. Journal of Climate, 28(1): 56–65, doi: 10.1175/JCLI-D-14-00438.1

Fogt R L, Bromwich D H. 2006. Decadal variability of the ENSO teleconnection to the high-latitude South Pacific governed by coupling with the Southern Annular Mode. Journal of Climate, 19(6): 979–997, doi: 10.1175/JCLI3671.1

Fogt R L, Bromwich D H, Hines K M. 2011. Understanding the SAM influence on the South Pacific ENSO teleconnection. Climate Dynamics, 36(7–8): 1555–1576, doi: 10.1007/s00382-010-0905-0

Gong Tingting, Feldstein S B, Luo Dehai. 2013. A simple GCM study on the Relationship between ENSO and the Southern Annular Mode. Journal of the Atmospheric Sciences, 70(6): 1821–1832

Gupta A S, England M H. 2006. Coupled ocean-atmosphere-ice response to variations in the southern annular mode. Journal and Climate, 19(18): 4457–4486, doi: 10.1175/JCLI3843.1

Kao H Y, Yu Jinyi. 2009. Contrasting eastern-pacific and central-pacific types of ENSO. Journal of Climate, 22(3): 615–632, doi: 10.1175/2008JCLI2309.1

L'Heureux M L, Thompson D W J. 2006. Observed relationships between the El Niño-Southern Oscillation and the extratropical zonal-mean circulation. Journal of Climate, 19(2): 276–287, doi: 10.1175/JCLI3617.1

Li Gang, Li Chongyin, Tan Yanke, et al. 2013. Impacts of the central and eastern Pacific types of ENSO on sea surface temperature in the South Pacific. Theoretical and Applied Climatology, 114(1–2): 315–327, doi: 10.1007/s00704-013-0840-1

Mcphaden M J, Zebiak S E, Glantz M H. 2006. ENSO as an integrating concept in earth science. Science, 314(5806): 1740–1745, doi: 10.1126/science.1132588

Mo K C, Higgins R W. 1998. The Pacific South American modes and tropical convection during the Southern Hemisphere winter. Monthly Weather Review, 126(6): 1581–1596, doi: 10.1175/1520-0493(1998)126<1581:TPSAMA>2.0.CO;2

Mo K C. 2000. Relationships between low-frequency variability in the Southern Hemisphere and sea surface temperature anomalies. Journal of Climate, 13(20): 3599–3610, doi: 10.1175/1520-0442(2000)013<3599:RBLFVI>2.0.CO;2

Philander S G H, Yamagata T, Pacanowski R C. 1984. Unstable Air-Sea interactions in the tropics. Journal of the Atmospheric Sciences, 41(4): 604–613, doi: 10.1175/1520-0469(1984)041<0604:UASIIT>2.0.CO;2

Saha S, Moorthi S, Pan H L, et al. 2010. The NCEP climate forecast system reanalysis. Bulletin of the American Meteorological Society, 91(8): 1015–1058, doi: 10.1175/2010BAMS3001.1

Sallee J B, Speer K G, Rintoul S R. 2010. Zonally asymmetric response of the southern ocean mixed-layer depth to the southern annular mode. Nature Geoscience, 3(4): 273–279, doi: 10.1038/ngeo812

Turner J. 2004. The El Niño-Southern oscillation and Antarctica. International Journal of Climatology, 24(1): 1–31, doi: 10.1002/joc.965

Yeo S R, Kim K Y. 2015. Decadal changes in the Southern Hemisphere sea surface temperature in association with El Niño-Southern Oscillation and Southern Annular Mode. Climate Dynamics, 45(11–12): 3227–3242, doi: 10.1007/s00382-015-2535-z

Yu J Y, Kao H Y, Tong L, et al. 2011. Subsurface ocean temperature indices for Central-Pacific and Eastern-Pacific types of El Niño and La Niña events. Theoretical and Applied Climatology, 103(3–4): 337–344, doi: 10.1007/s00704-010-0307-6

Yu J Y, Paek H, Saltzman E S, et al. 2015. The early 1990s change in ENSO-PSA-SAM relationships and its impact on southern hemisphere climate. Journal of Climate, 28(23): 9393–9408, doi: 10.1175/JCLI-D-15-0335.1

Zebiak S E, Cane M A. 1987. A model El Niño-southern oscillation. Monthly Weather Review, 115(10): 2262–2278, doi: 10.1175/1520-0493(1987)115<2262:AMENO>2.0.CO;2

Zhang Zhaoru, Uotila P, Stössel A, et al. 2018. Seasonal southern hemisphere multi-variable reflection of the southern annular mode in atmosphere and ocean reanalyses. Climate Dynamics, (3–4): 1451–1470